INVITED PAPER

Recording and Decoding for Neural Prostheses

This paper reviews technologies and signal processing algorithms for decoding peripheral nerve and electrocorticogram (ECoG) signals to interpret human intent and control prosthetic arms.

By David J. Warren, *Senior Member IEEE*, Spencer Kellis, *Member IEEE*, Jacob G. Nieveen, Suzanne M. Wendelken, Henrique Dantas, Tyler S. Davis, Douglas T. Hutchinson, Richard A. Normann, Gregory A. Clark, *Member IEEE*, and V. John Mathews, *Fellow IEEE*

ABSTRACT | This paper reviews technologies and signal processing algorithms for decoding peripheral nerve and electrocorticogram signals to interpret human intent and control prosthetic arms. The review includes a discussion of human motor system physiology and physiological signals that can be used to decode motor intent, electrode technology for acquiring neural data, and signal processing methods including decoders based on Kalman filtering and least-squares regressors. Representative results from human experiments demonstrate the progress that has been made in neural decoding and its potential for developing neuroprosthetic arms that act and feel like natural arms.

KEYWORDS | Brain–computer interface; electrocorticogram; Kalman decoders; neural decoding; neuroprosthetics; peripheral nerve signals

Manuscript received May 17, 2015; revised October 5, 2015; accepted November 19, 2015. Date of current version January 19, 2016. This work was supported in part by the Defense Advanced Research Project Agency (DARPA) under Award N66001-15-C-4017 and in part by the Space and Naval Warfare Systems Center Pacific (SSC Pacific) under Contract N66001-15-C-4017.

D. J. Warren, **S. M. Wendelken**, **R. A. Normann**, and **G. A. Clark** are with the Department of Bioengineering, University of Utah, Salt Lake City, UT 84112-9458 USA (e-mail: David.Warren@utah.edu; suzanne.wendelken@utah.edu; normann@utah.edu; Greg.Clark@utah.edu).

S. Kellis is with the Biology and Biological Engineering Division, California Institute of Technology, Pasadena, CA 91125 USA (e-mail: skellis@vis.caltech.edu).

J. G. Nieveen is with the Department of Electrical & Computer Engineering, University of Utah, Salt Lake City, UT 84112-9206 USA (e-mail: j.g.nieveen@utah.edu).

H. Dantas and **V. J. Mathews** are with the School of Electrical Engineering and Computer Science, Oregon State University, Corvallis, OR 97331 USA (e-mail: dantash@oregonstate.edu; mathews@oregonstate.edu).

T. S. Davis is with the Department of Neurosurgery, University of Utah, Salt Lake City, UT 84132 USA (e-mail: Tyler.Davis@hsc.utah.edu).

D. T. Hutchinson is with the Department of Orthopaedic Surgery, University of Utah, Salt Lake City, UT 84108 USA (e-mail: douglas.hutchinson@hsc.utah.edu).

Digital Object Identifier: 10.1109/JPROC.2015.2507180

I. INTRODUCTION

Limb amputation profoundly affects the activities of daily living. Although a substantial disability, individuals who have lost a limb retain the underlying neural circuitry and much of the ability to sense and control movements of their missing limb. That is, they have the ability to sense artificially evoked percepts and to control artificial limbs in manners similar to how they controlled their limbs prior to limb loss [1]–[15].

Prosthetic limbs have progressed in the last few decades from Civil War-era technology, such as cable-driven prostheses controlled by shoulder movements, to systems that use natural control signals to command their movements [16], [17]. Furthermore, highly dexterous robotic arm and hand prostheses have been sensorized to evoke meaningful artificial percepts for closed-loop control of their movements [18]–[22].

Paralysis resulting from spinal cord injury (SCI) and other diseases imparts a heavy burden on afflicted individuals, their families, and society. SCI damages only the connection between the brain and the periphery, leaving the brain intact and capable of planning movement, but destroying the bidirectional ability to relay motor and sensory information between the brain and the limbs. A wide range of assistive devices have been proposed for the SCI patients using interfaces that range from noninvasive, such as eye tracking, to highly invasive devices implanted into the brain. User acceptance of such devices is dependent upon the source of useful signals, the type of assistance provided, and the ease of use [23]–[26].

The key approach to treating both limb loss and paralysis is to use the ability of the nervous system to

generate movement commands in spite of the disabilities to restore function [9], [11], [27]–[33]. The goal of this paper is to describe representative technologies that may be used to interpret motor intentions from neural signals of the peripheral nervous system (PNS) and the central nervous system (CNS). In particular, this paper will review the use of action potentials recorded from the PNS, and the electrocorticogram (ECoG) recorded from the CNS. In addition to representing both single neuron and population-level neural activity, these two signals can be used in different ways for the two major patient populations that we address here: those with limb loss and those with paralysis.

II. AN OVERVIEW OF MOTOR SYSTEM PHYSIOLOGY

The nervous system plans and executes voluntary movements [34]–[36]. The source of the majority of the nervous system signals used for determining motor intent is the neuron, with the other cell type of the nervous system, glia, providing no information. As a result of electrochemical processes, a neuron can *fire* an action potential, an approximately 100-mV change in the potential within the neural cell relative to outside the cell, that lasts for approximately 1 ms. A neuron can have an axon, a part of the cell that projects away from the cell body, which can propagate action potentials to other neurons or to distal muscles and organs. Using an electrode located outside of the neuron, one can detect an action potential as a *spike* in the measured voltage.

Using the same electrode, one can record a continuously varying voltage that represents the average activity of many surrounding neurons [37]. Similarly, an electrode could be located on the surface of the neural tissue, too far away from individual neurons to detect individual spikes, but still close enough to measure the average synaptic activity or spike activity of neurons in the tissue below the electrode. These voltages represent the average signal produced by populations of neurons. These signals reflect the work of the corresponding neuronal populations as they process sensory inputs, produce motor outputs, or perform other functions.

The nervous system consists of the CNS, made up of the brain and spinal cord, and the PNS that contains nerves and ganglia. Neurons that serve similar functions are generally collocated in small regions within the CNS or the PNS. Neuron cell bodies in the CNS reside on the outer surface of the brain (cerebral cortex) or in deeper, subcortical structures containing collections of neuron cell bodies called nuclei. Ganglia are collections of neuron cell bodies in the PNS. Nerves contain axons whose cell bodies reside in ganglia or CNS.

Performing a movement involves three somewhat different but interrelated aspects: planning, preparation, and production (execution). These three aspects differently engage different neocortical motor regions: supplementary motor cortex, premotor cortex, and primary motor cortex, respectively. The distinctions are of practical importance for neural decodes, because planning and preparation can generate cortical spike activity comparable to that generated during the movement itself, even without the movement actually occurring. Neurons in premotor cortex fire during the preparation period much as they fire during the actual movement itself [38]. Similarly, supplementary motor cortical neurons can fire during both planning the movement and its later, delayed execution [39]. Thus, unlike the situation in nerve in which action potentials are effectively in a 1:1 correlation with muscle twitches, decodes of neural activity in cortex can lead to false positives that occur without actual movements. It is necessary for decodes to discriminate between movements that actually are to be generated, and movements that are only conceptualized.

The basal ganglia and the cortical motor regions receive sensory input from the neurons of sensory cortical regions and adapt the planning and preparation to the state of the limbs, hands, and the environment. Information about the intended movement is sent to the primary motor cortex, which initiates and indirectly executes the movement. During initiation, information regarding the planned movement is sent from primary and premotor cortices to the spinal cord and the cerebellum. The cerebellum supervises and adjusts the timing and performance of the movement based on sensory feedback.

Neural activity in primary motor cortex helps execute movements. In particular, the Betz cells of primary motor cortex, which produce large extracellular spike potentials, are active. The axons of these cells project to the spinal cord, communicating motor commands to the lower motor neurons that activate the muscles. The activity of individual neurons of primary motor cortex encodes production of force in a particular direction [40], [41], even if that force differs from the desired movement direction due to external forces [42]. However, the directional "tuning curve" for a single cortical neuron is broad, and there is a confound between the proximity of a movement to an individual neuron's preferred direction and the force level to be produced. Hence, recordings from many different cortical neurons are necessary to determine the population vector that more accurately encodes the movement [43]. Whether primary motor cortex encodes simple, muscle-related force production or the more abstract information of movement direction remains controversial and has resulted in active research on the neuronal code of motor cortex [44], [45]. Although simplified and incomplete, this description is adequate for our purpose.

The last neural step in the movement path is the lower motor neurons. These neurons have axons that project out to the skeletal muscles through the peripheral nerves. Each lower motor neuron innervates multiple

motor fibers (cells) in a single muscle. An action potential in a lower motor neuron results in a single muscle action potential in each of the muscle fibers innervated by the neuron, resulting in contraction of the muscle fibers. Often, axons of like purpose are collected together within the nerve into a fascicle, a collection of axons contained within an outer membrane sheath. A fascicle may contain axons of sensory neurons that relay information from the muscle contractions or skin sensory inputs back to earlier elements of the motor control path.

III. NEURAL SIGNALS AVAILABLE FOR DECODING

A. CNS Signals

1) Measurements of Action Potentials in Neurons: The most basic neural signal available for decoding is the spike event, the extracellular measurement of an action potential. To record such an event, one must place a recording electrode in close proximity to the desired neuron (within approximately 100 μm [46]). The organization of the tissue of cerebral cortex generally places the neurons of interest (e.g., Betz cells) 1–2 mm away from the surface of the cortex. Consequently, electrodes that penetrate into the cortex are necessary for recording these spike events. Spike events may be detected using voltage threshold or energy threshold methods, with the threshold tuned on a per-electrode basis to best capture neural activity from each electrode. When spike waveforms are recorded clearly enough to identify common stereotypical features, the spike events are called single unit activity (SUA), referring to the fact that the common features suggest a single neuronal source [47]. When spike waveforms can be separated from the noise, but do not have stereotypical features that identify a single neuronal source, the spike events are called multiunit activity (MUA). Both SUA and MUA have been widely studied in the context of neural prostheses, although single-unit spike firing rates are most commonly used [27]–[29], [31], [33], [48]. Spike classification allows calculation of the firing rate for each single unit source. However, the decoding improvement achieved by performing spike classification and using single unit firing rate data may not be significant [49]–[52].

2) Population Measures: In contrast to measuring spike events, the combined electrical activity of many neurons can also be recorded for neural prosthetic applications [37]. The nature of these recordings depends upon the size of the electrode and the separation between the electrode and neurons. The highest resolution population measure is the local field potential (LFP), which is sampled from the same electrode used to detect spike events. The lowest resolution population measure is the electroencephalogram (EEG), which measures brain activity from the scalp. The electrocorticogram, recorded at the cortical surface, strikes a balance between LFP and EEG in terms of invasiveness and spatial resolution. Cortical surface potentials may be further classified, based on the size and spacing of the recording electrodes, into spatio–temporal scales ranging from macro-ECoG, recorded with standard clinical grids, to micro-ECoG (μECoG), recorded with smaller, denser grids of electrodes. Although population measures are less specific than spike events, they are more robust to micromotion, foreign body responses, and other time-varying parameters that interfere with recordings of action potentials [53]–[55]. Because of these advantages, population measures represent an attractive option for long-term brain–machine interfaces [53]–[67]. In particular, ECoG signals have seen a surge of interest recently [68]–[81].

B. PNS Signals

Spike events may also be recorded from neurons in the PNS using penetrating electrodes placed based on the organization of the PNS. For example, to gain access to the nerves that innervate the finger flexor and extensor muscles, the electrodes should be placed between the spinal cord and the point at which the small nerve branches leave the nerve trunk (in the middle upper arm). Because the nerve trunks are reorganized in the brachial plexus (approximately at the armpit level), the ideal location is between the middle of the upper arm and the armpit. Because PNS spike events may reflect either muscle contractions or sensory inputs, decoders must be designed to retain motor-related signals and reject sensory signals.

The electroneurogram (ENG) represents activity of a population of neurons in the PNS, and is similar to CNS LFP. Because nerves consist of axons leading from neurons to muscles, the intrafascicular ENG represents direct control signals rather than population interactions. There are many more studies using nonpenetrating electrodes in the PNS than with penetrating electrodes. However, most of such works decode sensory activity, not motor activity [82]. ENG measured at the skin surface is obscured by electromyograms (EMG) arising from muscles and is not typically used for neural decoding.

C. EMG Signals

Although technically EMG is not a neural signal, we briefly mention it as they are used in commercially available, state-of-the-art myoelectric prostheses [8]. Given muscle loss from amputation and, if not lost, the limited ability to separate the contribution of each muscle in the surface EMG signal, each degree of freedom (DoF) of movement is not necessarily controlled with a homologous muscle. Furthermore, complex movements require mode switching, where an EMG signal is mapped to different movements during different phases of the overall movement. Although patients can become quite adept with their

myoelectric prosthesis, the control is not intuitive. EMG signals are discussed elsewhere in this issue [83].

IV. ACQUISITION OF NEURAL SIGNALS

Table 1 contains a summary of commonly encountered devices for acquiring neural signals.

A. Recording Spike Events

Electrodes that record spike events typically have a small surface area (200–34 000 μm^2 [84]) and high impedance (10–300 kΩ, measured at 1 kHz). Microelectrode arrays are typically used to record spike events and wide-band signals from multiple sites within a cortical or peripheral nerve region. For cortical recording, commonly encountered array designs are the Utah electrode array (UEA) [85], commercially available from Blackrock Microsystems, the Michigan Probe in both 2-D [86] and 3-D [87] format, commercially available from NeuroNexus, and the microwire probe [88], commercially available from multiple sources. The largest difference between these devices is that the UEA and the microwire arrays measure neural activity from a single sensor site on each shaft or microwire, whereas the NeuroNexus 2-D probe measures neural activity at multiple depths of cortex along the axis of the electrode.

Peripheral nerve recording devices can be separated into those that record at the surface of nerves and those that penetrate into the nerves. Surface recording nerve electrodes are typically called cuff electrodes as they act as a cuff wrapped around the nerve. A variant of the cuff electrode is the flat interface nerve electrode (FINE), which flattens the nerve so that electrodes are in closer proximity to the nerve's fascicles [89]. Although signal processing attempts have been made to improve the recording performance of cuff electrodes [90]–[92], they have found more success as stimulating interfaces. Two basic designs exist for penetrating electrodes. The longitudinal intrafascicular electrode (LIFE) is an insulated conductor that has a small deinsulated region [93]. This

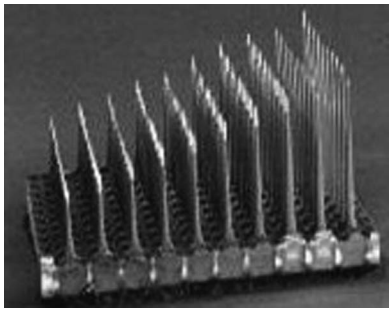

Fig. 1. *The USEA is a neural recording and stimulating device targeted toward implantation in peripheral nerves. At the tip of each of the 100 shafts is a metal electrode (platinum or iridium–oxide) that can record both spike events and ENG data. The lengths of the shafts vary between rows so that the electrode can reach nerve fibers at different depths from the surface of the nerve. Each electrode shaft is isolated from other shafts with glass moats and the entire device (except at the electrodes) is insulated (presently via Parylene-C).*

device is threaded into a nerve in such a manner that the exposed region rests within a fascicle to record spike events. The design has since been adapted to allow for multiple electrodes along the length of the LIFE [94]. A similar design, the transverse intrafascicular multichannel electrode (TIME), threads a multisite interface from one side of the nerve to the other [95]. A recording device similar to the UEA is the Utah slanted electrode array (USEA) (Fig. 1) [96]. By using shafts of different lengths for each row, the electrodes can reach nerve fibers at different depths from the nerve surface.

B. Recording Neural Population Activity

As an alternative to recording spike events, one can record wide-band signals to obtain LFP, ECoG, EEG, or ENG signals. Whereas spike events reside in the higher frequency bands of the wideband intracortical recording (i.e., > 1000 Hz), these other signals are typically extracted from the lower frequencies (the upper limit

Table 1 List of Neural Interfaces Discussed

Neural Interface	Abbreviation	Implant Site	Neural Signal Recorded
Utah Electrode Array	UEA	Cerebral Cortex	Spike Events
Michigan Probe		Cerebral Cortex	Spike Events
Microwire Probe		Cerebral Cortex	Spike Events
Cuff Electrode		Extraneural Peripheral Nerve	Population Activity
Flat Interface Nerve Electrode	FINE	Extraneural Peripheral Nerve	Population Activity
Longitudinal IntraFascicular Electrode	LIFE	Intrafascicular Peripheral Nerve	Spike Events
Transverse Intrafascicular Multichannel Electrode	TIME	Intrafascicular Peripheral Nerve	Spike Events
Utah Slanted Electrode Array	USEA	Intrafascicular Peripheral Nerve	Spike Events
Electrocorticogram Array	ECoG	Surface of Cerebral Cortex	Population Activity
μElectrocorticogram Array	μECoG	Surface of Cerebral Cortex	Population Activity

decreases as the signal is recorded further from the neural sources; thus, for intracortical LFP it may be < 500 Hz whereas for EEG it may be < 50 Hz).

Cortical surface potentials have been recorded using a wide variety of electrodes, from large grids with 5-mm diameter electrodes and 1-cm spacing to small grids with <100-μm diameter electrodes and 1-mm spacing (Fig. 2). Larger populations of neural sources must act with greater synchrony to change the electric potential of a large electrode. Smaller electrodes may experience voltage fluctuations due to the activity of smaller populations. Thus, depending on the electrode used to sample the cortical surface potential, the spatial resolution of the ECoG signal may range from submillimeter to centimeter scales [69], [97]–[99]. To expand coverage of the cortical surface, several researchers have integrated multiplexing and buffering electronics into the array, increasing electrode counts from several tens to several hundreds [71], [100].

C. Longevity and Stability of Neural Recording

The value of a neural interface as the basis of a neuroprosthesis is highly dependent upon the longevity and stability of the device. Ideally, the neural interface should provide useful recordings for many years. Furthermore, the information associated with the activity measured on each electrode ideally should remain constant over the life of the device.

Of the neural interfaces that record spike event data, the UEA has the largest body of literature regarding its longevity. Even three years post-implant, the device was able to record spike event data from human motor cortex [101]. Further, it has been reported that some neurons in motor cortex can be recorded by a UEA for more than 100 days [102]. Although not yet correlated to *in vivo* performance, a recent study compared the longevity of multiple devices during *in vitro* exposure to reactive accelerated aging solutions and found all devices exhibited degraded performance [103]. Due to the comparatively fewer number of implants, there is much less data available for devices that record spike events in the PNS. The USEA has been reported to record neural activity for up to four months in cat [10] and LIFE devices have been reported to record spike events for up to six months in cats [104].

Several studies have demonstrated the relative stability of ECoG signals both in the short term, i.e., within session, and the long term, i.e., over days and months [105], [106]. Longevity studies in humans are difficult due to FDA regulations limiting experimental implants to 30 days or fewer. One device study in rat found minimal histological response to implanted surface electrodes after 25 weeks [107]. Although there have been no rigorous studies of ECoG device longevity, the materials used in most standard clinical ECoG electrodes—platinum and silicone—are frequently used in implantable devices due to their biocompatibility.

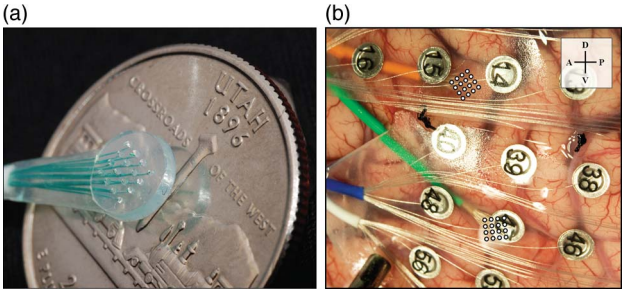

Fig. 2. ***ECoG and μECoG devices. (a) A single 16-electrode 4 × 4 μECoG grid shown next to a U.S. quarter-dollar coin. (b) Photograph of ECoG and μECoG in vivo*; the green and blue wire bundles lead to the μECoG arrays over Wernicke's and face-motor cortex, respectively; the larger silver disks are ECoG electrodes. Reproduced with permission from [69].**

V. SIGNAL PROCESSING FOR NEURAL DECODING

In this section, we discuss how one performs human subject research on decoding movements and briefly describe the two most commonly encountered approaches, classification of the movement into one of a finite set of possible movements and continuously estimating the intended movement.

A. Experimental Construct for Neural Decoding

Fig. 3 illustrates the process of decoding neural signals for prosthetic control. Neural signals are acquired via one or more electrodes and then preprocessed to mitigate the effects of external interferences and measurement noise as well as crosstalk among the electrodes. The enhanced signals are then processed to extract a number of features that will be used to estimate the intent of the subject. These features, or the enhanced signals themselves, are analyzed during training to select the appropriate channels for decoding the movement information. Features derived from the selected channels are used to perform the decoding task. The output of the decoder is used to control the prosthetic device.

B. Overview of Decoding Approaches

1) Discrete Decoders: Discrete decoders classify movements into one of a finite number of possible movements, such as a complex hand shape that represents a particular grasp. Several variations, including those employing linear discriminant analysis, support vector machines, and artificial neural networks, have been explored with EMG signals [30], [108]–[115]. Discrete decoders

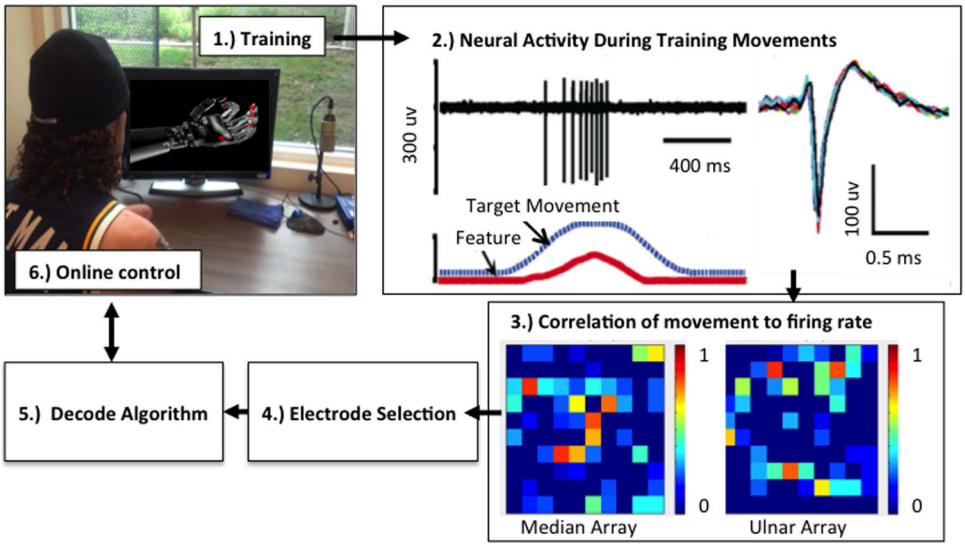

Fig. 3. ***Schematic diagram of PNS recording and decoding in an experimental set up. 1) Data is collected from the subject's nerves while the subject performed desired movements with his phantom hand. 2) Spike times are recorded and converted into firing rates. (Feature selection) 3) Firing rates for each channel are correlated with the intended movement amplitude during training. 4) Electrode channels with high correlation between firing rate and intended movement are chosen as inputs to the decode algorithm. Other approaches to channel selection are possible. 5) Data from several trials of selected movements and electrodes are used to train the decode algorithm. 6) Control of the selected movements of the prosthetic hand (virtual hand in this figure) is turned over to the subject.***

are commonly used to identify motor intention from ECoG signals [74], [116]–[119], and from PNS signals [9], [12], [120], [121]. Although classifier methods are useful in certain scenarios, such methods can only evoke a limited set of predefined movements.

2) Continuous Decoders: Continuous decoders create a movement estimate that continuously varies over the range of possible movements. Continuous decoders using ECoG signals have been demonstrated in a number of neural prosthetic applications. Early studies used motor and speech imagery to control up to 2 DoFs [122], [123]. Arm and hand movements, including observation, onset and execution, and imagination, have been successfully decoded from ECoG [76], [124]–[126]. Movements of individual fingers have also been decoded [127]–[129]. ECoG was recently investigated in a human with tetraplegia [75], [81]. Bayesian methods, such as Kalman decoders, were used in the majority of these works.

Comparatively few researchers have reported continuous decoder performance with recordings from intrafascicular electrodes implanted in humans. Dhillon and Horch reported a proportional 1-DoF control of a computer cursor using LIFE implants in the median and ulnar nerves of the upper arm [1]–[3]. Warwick *et al.* reported the performance of a proportional decoder using signals from a Utah Electrode Array implanted in the ulnar nerve of a subject with intact hands [130]. Several of this paper's authors have been testing USEAs implanted in the median and ulnar nerves of human amputees for restoring motor and sensory functions [13].

VI. SIGNAL ENHANCEMENT

There is often substantial overlap in the information recorded by groups of electrodes of the interface. Furthermore, common noise elements often appear on all electrodes.

For peripheral nerve recording devices, EMG signals from nearby muscles often appear in the recorded signals on all channels (e.g., [10]). The common average reference (CAR) method is commonly used to reduce this noise. In this approach, the mean of the signals acquired by all the electrodes at each sampling instant is used as a *virtual reference* that is subtracted from the signal recorded by each electrode [131], [132]. Fig. 4 shows how this method mitigates the effect of EMG present in recordings from a USEA implanted in a human peripheral nerve. The CAR approach can be generalized to spatially varying virtual references by defining a neighborhood of adjacent electrodes over which to average [133]–[135].

Some sources of distortion produce transient artifacts that can be discarded when they cross a specified threshold or may need to be identified and discarded manually. Other distortions produce slow shifts in baseline voltage that can be removed by detrending the signal [136]. Oscillatory noise sources can be attenuated using bandstop, notch or comb filters centered on the noise frequency (and harmonics). The characteristics of these

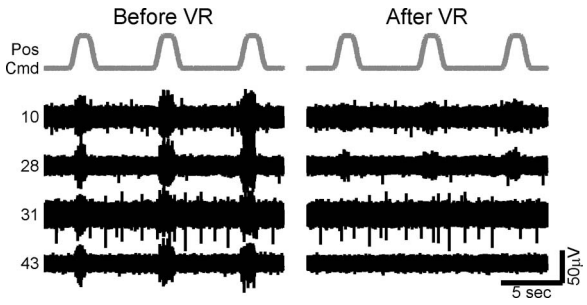

Fig. 4. *(Left) Raw recordings from four USEA electrodes implanted in a human peripheral nerve. When the implanted volunteer attempts to track the commanded finger position (Pos Cmd) shown at the top of the panel, all four electrodes exhibit simultaneous activity that is most likely EMG. (Right) The same four channels over the same time epoch after applying a virtual reference. In the right panel the spike events (appear as impulses in this time scale) are clearly detectable on electrode 31. In contrast, electrode 43 contains no valuable information [13].*

interferences often change over time, and adaptive methods may be necessary in such situations [137].

VII. FEATURE SELECTION

The raw measurement of action potentials from the CNS or the PNS is rarely used directly for decoding of movement intentions. This section presents two methods for extracting informative features associated with the action potentials.

Neural spikes are typically detected from the measured data using some form of thresholding, and may also be sorted based on the spike waveform [47]. The simplest feature one can extract from the detected spike times is the firing rate estimated by counting the number of detected spikes and dividing by the time interval over which the data was collected. Spike firing rates range from 0 to 1000 spikes/s, although sustained firing rates above 100 spikes/s are unusual for motor-related neurons.

A common feature for decoding behavior from population signals is the power in discrete frequency bands. Phase information has also been used in decoding applications [124], [138], [139]. Fig. 5 analyzes the variation of spectral power over time for μECoG signals acquired by two electrodes, one located over the Wernicke's area and the second over the face motor cortex (FMC), during a period of conversation followed by the subject repeating the word "yes" multiple times. FMC is responsible for the muscular control of speech. Wernicke's area processes language more abstractly. It can be seen from the figure that the time-frequency distribution as well as the mean signal power of the frequency range [70, 200] Hz modulates differently for conversation versus rote repetition.

VIII. CHANNEL SELECTION/ COMPLEXITY REDUCTION

One difficulty with multichannel neural signal processing is the amount of data that must be processed. For example, in the PNS signal analysis presented in Section X, there were 192 recorded channels of data. These large data sets may include linear dependencies as well as channels which generate erroneous predictions, in addition to the channels which produce the desired outputs [140]. This section reviews common methods for reducing this complexity by determining the most important channels or features needed to achieve satisfactory results.

A. Correlation-Based Channel Selection

The simplest and the most common method for channel selection is to pick the signals in the neural channels that are most correlated with the hand kinematics signals. The correlation coefficient of two real-valued scalar signals $x(t)$ and $y(t)$ is given by

$$c_{xy}(t) = \frac{\left|E\{x(t)y(t)\}\right|}{\sqrt{E\{x^2(t)\}E\{y^2(t)\}}} \tag{1}$$

where $E\{(\cdot)\}$ represent the statistical expectation of $(\cdot)$. Assuming ergodicity, we can replace the statistical expectation with time averages within the training set. Although this is a simple approach, it does not provide a mechanism for eliminating redundant channels that contain the same information.

B. Mutual-Information-Based Channel Selection

Mutual information of two random variables measures how much information one variable contains about the other. The joint mutual information of N random variables is defined as

$$I(X_1, X_2, \ldots, X_N) = \int_{x_1}\int_{x_2}\cdots\int_{x_N} f_{X_1,X_2,\ldots,X_N}(x_1, x_2, \ldots, x_N) \times \log\frac{f_{X_1,X_2,\ldots,X_N}(x_1, x_2, \ldots, x_N)}{f_{X_1}(x_1)f_{X_2}(x_2)\cdots f_{X_N}(x_N)}\,dx_1dx_2\cdots dx_N \tag{2}$$

where $f_X(x)$ denotes the probability density function of the random variable X. Joint density functions are defined similarly. Larger values of joint mutual information indicate that the members of the set of random variables can be estimated with small errors using the other members in the set. Thus, one way to select L neural channels for decoder use is to compute the joint mutual information between the hand kinematics signals and the neural signals associated with all possible combinations

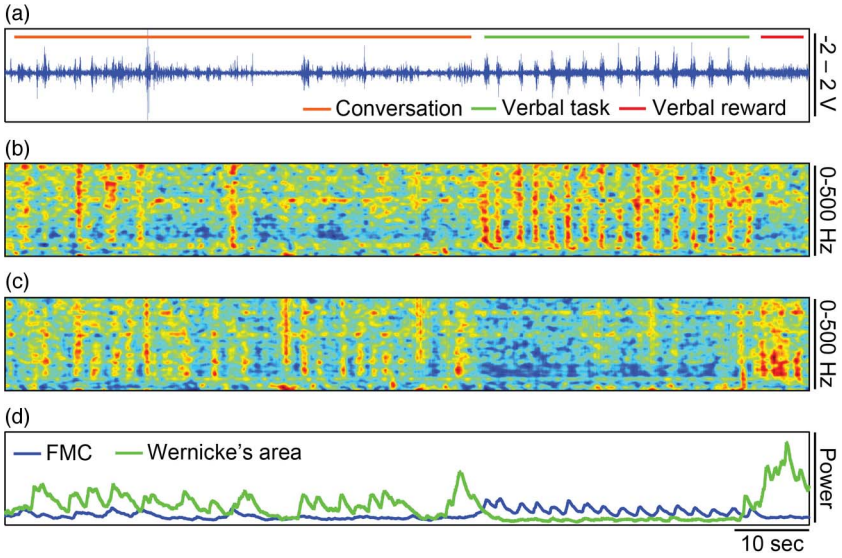

Fig. 5. ***Raw data, spectrogram, and mean power of ECoG signals in two different channels during conversation and a verbal task. (a) Audio waveform of conversation and verbal task in which the patient repeated the word "yes." (b) Normalized spectrogram of neural data recorded from a single electrode over FMC during the same time period shown in (a). (c) Normalized spectrogram of neural data recorded from a single electrode over Wernicke's area during the same time period shown in (a). (d) Mean power between 70 and 200 Hz for the 16 electrodes over FMC and the 16 electrodes over Wernicke's area. Notice the differences between (b) and (c) as the activities change. The two plots in (d) also shows similar differences based on the activity at any time. Reproduced with permission from [69].***

of L neural channels, and then to pick the set of L channels with the highest joint mutual information.

This approach is probabilistic and does not depend on the decoder model. A high value of mutual information indicates the existence of a possibly nonlinear decoder that will estimate the hand kinematics accurately. However, probability density functions are rarely available, and must be estimated from training data. Reliable estimation of high-order joint probability functions requires large data sets. A suboptimal method that employed the joint mutual information of fewer numbers of neural channels than required for the optimum approach was presented in [141] and showed promising decoder results.

C. Principal Component Analysis

Principal component analysis (PCA) [142] produces a transformed data set whose members are uncorrelated with each other through eigenanalysis techniques. When signals in the original data set are highly correlated, the eigenvalues of the correlation matrix of the data set exhibit large disparity, and in such cases a few "principal components" (i.e., the transformed signals) of the signal set may adequately represent the information content in all channels in the neural data set, resulting in reduced complexity of the decoder. It is also possible to perform a correlation analysis of the principal components of neural signals with the hand kinematics data to provide additional improvements in decoder efficiency and performance.

One advantage of PCA is that it is implemented in common software libraries. However, PCA only creates uncorrelated components, not independent components. Independent component analysis (ICA) [143] is an alternate technique that may be used to produce transformed signal sets whose members are independent of each other.

IX. NEURAL DECODING ALGORITHMS

A wide variety of algorithms have been applied to the problem of inferring behavior from neural recordings. These include, but are not limited to, neural networks, discriminant analysis, Bayesian methods, Gaussian models, perceptrons, hidden Markov models, support vector machines, linear regression, and Kalman filters (for a review, see [144]). We consider only two common approaches here: Kalman decoding and least-squares regression-based methods. These methods can be applied to any of the features used by the decoder.

Let $\mathbf{x}_k$ be a $M \times p$-element state vector containing the most recent p instances of some representation of the desired hand position at time k. Let $\mathbf{X}_k = [\mathbf{x}_1, \mathbf{x}_2, \ldots, \mathbf{x}_k]^T$ be the data matrix containing the hand kinematic state history from time t_1 through t_k, where the superscript T denotes matrix transpose operation. Similarly, let

$$\mathbf{z}_k = [z_1(t_k - d_1)\ z_2(t_k - d_2)\ \cdots\ z_C(t_k - d_C)]^T \quad (3)$$

represent a C-element vector of observations at time t_k for the decoder. The entries of this vector are the features extracted from the current and most recent L samples of data recorded from the electrode array. This representation acknowledges the time lag between a person's intent and the actual action. The time delay d_m between the mth entry of $\mathbf{z}_k$ and the hand position may be different from the delays associated with every other entry. Let $\mathbf{Z}_k = [\mathbf{z}_1, \mathbf{z}_2, \ldots, \mathbf{z}_k]^T$ represent the data matrix containing the observation vectors until time k.

A. Regression-Based Decoders

Regression-based decoders fit the parameters of a model that relates neural signal features to the hand kinematics as in

$$\widehat{\mathbf{x}}_k = f\{\mathbf{z}_k, \mathbf{W}\} \tag{4}$$

where f is a possibly nonlinear function completely described by the variables in the parameter vector $\mathbf{W}$. The goal during training is to determine the values of $\mathbf{W}$ such that some nonnegative cost function of the decoding error $\mathbf{x}_k - \widehat{\mathbf{x}}_k$ is minimized. As an example, we consider the least squares (LS) cost function given by

$$J = \sum_{k=1}^{M} \left(\mathbf{x}_k - f\{\mathbf{z}_k, \mathbf{W}\}\right)^2 \tag{5}$$

where M is the number of sample vectors in the training data. For a linear or linear-in-the-parameter nonlinear system model where the decoder output can be written as

$$\widehat{\mathbf{x}}_k = \mathbf{W}\mathbf{z}_k \tag{6}$$

the LS estimation has a closed-form solution given by

$$\widehat{\mathbf{W}} = \left(\mathbf{Z}_M^T \mathbf{Z}_M\right)^{-1} \left(\mathbf{Z}_M^T \mathbf{X}_M\right). \tag{7}$$

For most other system models, iterative approaches are needed.

B. Kalman Decoding

The Kalman framework has been extensively used for neural decoding [145]–[147]. For this discussion, we assume that the temporal evolution of the state vector is linear, and given by

$$\mathbf{x}_{k+1} = \mathbf{A}\mathbf{x}_k + \mathbf{w}_k \tag{8}$$

where $\mathbf{w}_k$ is the prediction error vector that is assumed to be Gaussian with zero mean value and covariance matrix $\mathbf{W}$, and $\mathbf{A}$ is the predictor matrix for the state vector. Similarly, we assume a linear generative model that relates the neural signal $\mathbf{z}_k$ to the state vector $\mathbf{x}_k$ as

$$\mathbf{z}_k = \mathbf{H}\mathbf{x}_k + \mathbf{q}_k \tag{9}$$

where $\mathbf{q}_k$ is the modeling error vector that is assumed to be Gaussian with zero mean value and covariance matrix $\mathbf{Q}$, and $\mathbf{H}$ is the coefficient matrix.

In the context of motor disability, we do not have information about hand kinematics available. This is the information that the decoder attempts to estimate. The Kalman decoder problem then becomes that of estimating the state vector $\mathbf{x}_k$ at time t_k given the observation vector $\mathbf{z}_k$, knowledge of the coefficient matrices $\mathbf{A}$ and $\mathbf{H}$ along with the noise covariance matrices $\mathbf{W}$ and $\mathbf{Q}$. Table 2 describes the process of iteratively estimating the hand kinematics vector [145]. The iterations are initialized with $\mathbf{P}_0 = [0]$, $\hat{\mathbf{K}}_0 = [0]$, and $\hat{\mathbf{x}}_0 = [0]$, where the matrix $[0]$ is a matrix of zeros with appropriate dimensions.

The matrices $\mathbf{A}$, $\mathbf{H}$, $\mathbf{W}$, and $\mathbf{Q}$ are in general not known *a priori* and must be estimated. Furthermore, since disabled persons cannot move a natural limb, we need to find another way of estimating the unknown parameters. One way to train the algorithm in this situation is to externally control a robot hand or a virtual hand to achieve desired motion, and to use the kinematics associated with the virtual or robot hand in place of the hand kinematics. The subject or patient will then be asked to follow in his/her mind the movement of the virtual hand with his/her disabled or missing hand. Once the data are acquired, we can use an LS or another similar approach to estimate the unknown parameters from the training data [148]. During normal operation of the Kalman decoder (i.e., outside the training set), we keep the estimated values of the above four matrices fixed while the other variables in the algorithm are iteratively updated as shown in Table 2.

C. Extensions

The regression-based decoder formulation is general and accommodates linear and nonlinear systems including kernel-based nonlinear decoders such as those described in [149].

A number of improvements have been proposed to adapt Kalman decoders, and several of these have been evaluated in [148]. Gilja *et al.* proposed several changes to the way in which the Kalman filter is parameterized to explicitly recognize the presence of a user interacting with the system [147]. Mulliken *et al.* incorporated goal information in the Kalman filter model [150]. A

Table 2 Kalman Filter Update Equations

A *priori* state update:	$\hat{\mathbf{x}}_k^- = \hat{\mathbf{A}}\hat{\mathbf{x}}_{k-1}$
A *priori* error covariance matrix:	$\mathbf{P}_k^- = \hat{\mathbf{A}}\mathbf{P}_{k-1}\hat{\mathbf{A}}^T + \hat{\mathbf{W}}$
Kalman gain:	$\mathbf{K}_k = \mathbf{P}_k^-\hat{\mathbf{H}}^T(\hat{\mathbf{H}}\mathbf{P}_k^-\hat{\mathbf{H}}^T + \hat{\mathbf{Q}})^{-1}$
State update:	$\hat{\mathbf{x}}_k = \hat{\mathbf{x}}_k^- + \mathbf{K}_k(\mathbf{z}_k - \hat{\mathbf{H}}\hat{\mathbf{x}}_k^-)$
Error covariance matrix:	$\mathbf{P}_k = (\mathbf{I} - \mathbf{K}_k\hat{\mathbf{H}})\mathbf{P}_k^-$

recursive maximum likelihood method was presented in [151]. Others have explored nonlinear techniques including generalized additive models, neural networks, and global Laplacian models [152]–[155].

An efficient design of a Kalman decoder with a nonlinear but a linear-in-the-parameter generative model was introduced in [141]. This work considered a generative model of the form

$$\mathbf{z}_k^{(nl)} = \mathbf{H}^{(nl)}\mathbf{x}_k + \mathbf{q}_k^{(nl)} \tag{10}$$

where $\mathbf{z}_k^{(nl)}$, the observation vector is made up of linear and nonlinear functions of the elements in $\mathbf{z}_k$. The number of elements in $\mathbf{z}_k^{(nl)}$ may be different from that in $\mathbf{z}_k$. For this generative model and the temporal state evolution model in (8), the structure of the Kalman decoder algorithm is identical to that for the linear generative model in (9).

X. RESULTS OF HUMAN EXPERIMENTS

After receiving approvals from the Institutional Review Board and informed consent from the subjects, four amputee subjects were implanted with one or two USEAs. Two other subjects were implanted with two 16-channel ECoG electrode arrays while undergoing surgery.

A. Experiments With PNS Signals

The results presented here are for a single amputee subject. This subject was implanted with two USEAs in the median and ulnar nerves (one per nerve). These are two of three nerves that control the movements of the fingers and the wrist. Each array was referenced to a locally placed, low-impedance wire. The 192 channels of data were bandpass filtered (750 Hz to 7.5 kHz) and sampled at 30 kHz. Spike detection was performed using voltage thresholding, set to six times the RMS value for each channel. The firing rates were calculated over 33 1/3-ms intervals and smoothed with a 300-ms-long rectangular FIR filter. The smoothed firing rate was used as the input to the decoders. Decode methods and associated parameters were calibrated using training data and subsequently tested in real time. Offline *post hoc* training and testing was also performed.

Online decoding was performed in a virtual environment (Musculoskeletal Modeling Software [156]). The virtual hand was modeled as having movement in 12 DoFs, including flexion and extension of each digit (5 DoFs), adduction and abduction of all except for the third digit (4 DoFs), and wrist roll, pitch and yaw (3 DoFs). Joints of individual digits were coupled to appear as a single DoF.

During training, the subject was instructed to track the movement of a simulated hand with his imaginary (phantom) hand while the firing rates of all 192 USEA electrodes were recorded. The instructed movement followed a semi-sinusoidal path over a range and at a velocity deemed comfortable by the subject. Only movement of a single DoF was instructed during each training trial and multiple ($\geq$11) training trials of each movement were performed. To train multi-DoF decoding methods, movement trials for each DoF were concatenated.

During testing, the instructed movements were provided by semitransparent spheres and the decoded hand position was shown as the position of the virtual hand. The subject's task was to move his phantom hand such that the tips of each virtual finger and the virtual wrist position tracked the position of the spheres, with one sphere for each finger and another for the wrist. For most trials, only one of the spheres moved in only one of the above listed DoF while the remaining spheres were held stationary. The moving sphere(s) followed a semisinusoidal path at a velocity similar to the training trials. The color of each sphere, whether moving or stationary, was green or red, depending upon whether the difference between the decoded and instructed fingertip position was within 5% of the available range of motion or outside that range, respectively. In separate testing trials, the spheres jumped to new positions and the subject's task was to move and hold stationary his phantom hand such that the virtual fingertips and the virtual wrist were in the instructed position of the spheres. In these trials, both individual DoF movement and combination movements of multiple DoFs (e.g., thumb-index finger pinch) were tested. Typically, between 3 and 6 different DoFs were simultaneously tested for either tracking or move tasks.

1) Offline Assessment: Fig. 6 shows a comparison of the distribution of the correlation coefficient between the estimated and desired movements for four different

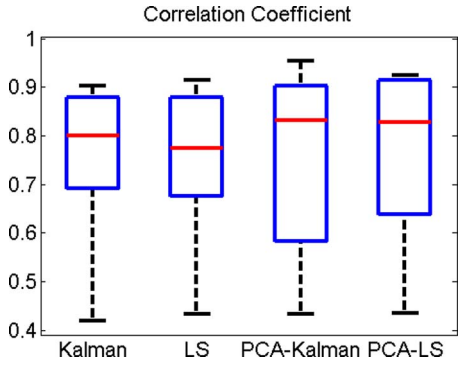

Fig. 6. ***Box plots of the correlation coefficient of the estimated and the desired finger movements. Although the average behavior of the PCA-based decoders is slightly better than that of the other methods, they exhibit higher variability.***

decoders using all possible data sets obtained from one of the subjects. The four methods included a linear regressor and a Kalman decoder along with PCA-based versions of these methods. The Kalman and the LS regression-based decoders used a linear model employing up to 30 channels and ten-sample memory. For each DoF, ten channels were selected to be used as predictors via a correlation analysis during training. The resulting channels for all 3 DoFs (up to 30 channels in all) were combined into a single pool of predictor sources and used by the decoder for estimating each movement. The PCA-based decoders used the ten principal components that best represented the information contained in the same pool of neural channels, using ten samples of memory.

Fig. 7 shows a comparison of the decoder outputs in one of the experiments. Only movement of the thumb, index, and ring fingers are examined here. The results indicate that all the methods performed similarly, and tracked the virtual arm with small errors. Although the PCA-based methods performed slightly better on average, they exhibited higher variability. During the movement of one finger, the other fingers were commanded to be still. To assess how well this goal was achieved, we estimated the correlation coefficients of the estimated movement of each finger with the desired movements of all three fingers. The maximum value of the correlation coefficient between different fingers in all the experiments was 0.16 and in almost all cases below 0.07. Based on the above observations, the remainder of this section only presents results for the basic Kalman decoder.

Fig. 8 demonstrates the performance of the Kalman decoder as a function of the number of DoFs of the decoder. In general, the performance suffers as the simultaneous DoF decoded increases. Nevertheless, the majority of the correlation coefficients exceeded 0.5. These results were obtained by considering all possible training data sets and all possible combinations of the DoFs.

2) Online Decoding: An example of the performance of a real-time Kalman decoder is shown in Fig. 9. The top three traces in the figure show the requested movement (solid black line) and the estimated movement (dashed colored lines) for individual movements of thumb, index, and ring fingers. As was the case during offline analyses, the decoder estimated the movements correctly with small errors. The bottom panel of the figure shows the times of spike events in six different electrodes as vertical bars. One can readily observe that each finger's movement resulted in a unique pattern of activity.

B. Experiments With ECoG Signals

The data used in this experiment were collected from a patient undergoing ECoG recordings prior to the surgical treatment of epilepsy [76]. The patient was implanted with two 16-channel nonpenetrating microwire arrays that consisted of 40-μm wires embedded in a silicone

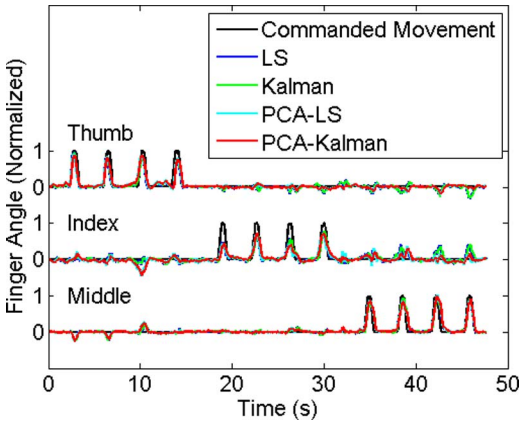

Fig. 7. ***Comparison of the estimated and the desired finger movements for four different linear decoding methods. The decoders estimated the movements with small errors. No method substantially outperformed the others.***

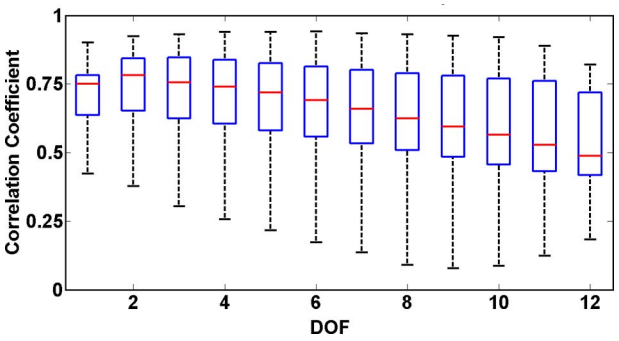

Fig. 8. ***Box plots of the correlation coefficients of the estimated movements with the desired movements as a function of the DoFs used by the decoder.***

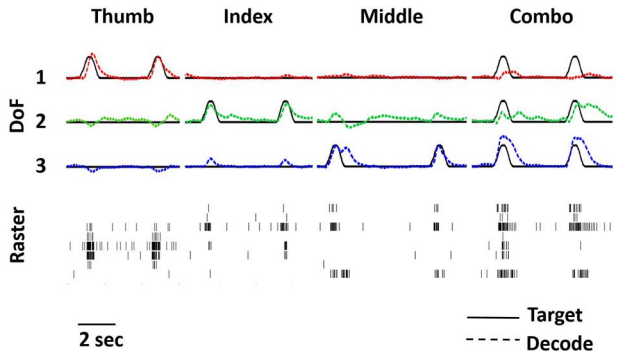

Fig. 9. *Example of testing of a previously trained Kalman decoder. The top three traces depict the target location (solid black line) and the subject-controlled virtual finger location (dashed colored lines) for individual movement of the thumb, index, and middle fingers. The lower panel shows a raster plot of the times of spike events from six selected electrodes during this task.*

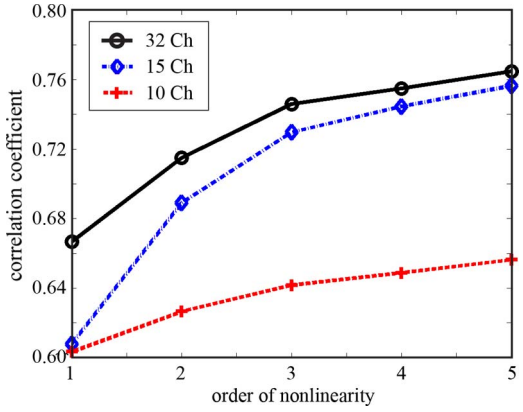

Fig. 10. *Correlation coefficients of the measured and estimated hand movements in the ECoG experiments. The nonlinearity order of the model ranged from 1 (linear) to 5. The performance penalty for using only 15 channels may not be substantial while ten channels may not be sufficient [141].*

substrate with 1-mm interelectrode spacing (PMT Corporation, Chanhassen, MN, USA). The arrays were placed in the epipial space underneath a standard clinical electrocorticographic (ECoG) grid. One of the arrays was placed over the arm and hand representations in motor cortex. Both arrays were referenced to low-impedance wires placed in the epidural space. The patient performed a reaching task using a mouse on a draftsman tablet (20 cm $\times$ 20 cm). Thirty two channels of neural data and two channels of x and y hand position data were recorded at 30-kHz sampling rate. Because hand movements are low frequency signals, our system preprocessed the hand and neural signals using a low-pass filter with 10-Hz cutoff frequency and subsampled the resulting signals at the rate of 60 samples/s. The data were broken into seven parts. The Kalman decoder was trained on the first part and tested on the other six.

Fig. 10 demonstrates the performance of the Kalman decoder under a variety of system configurations. The figure displays the correlation coefficients between the estimated and measured hand movements (averaged over the six test blocks). The generative model employed in the Kalman decoder varied from a purely linear system (nonlinearity order $= 1$) to a polynomial nonlinearity of order 5. The system employed a constant delay, estimated from the training data, between the neural signals and the hand movements. All systems considered here employed a five-sample memory. The comparisons also included the case of a reduced number of channels selected through mutual information-based analysis.

The nonlinear model outperformed the linear model in these experiments. Reducing the number of channels to 15 from 32 did not result in a substantial loss of performance, indicating that the mutual information-based approach performed as desired and that there may be substantial overlap among the information recorded by different electrodes. Fig. 11 displays the measured and estimated hand movements for the fifth-order nonlinear model using 32 and 15 channels and five-sample memory. We can see that the Kalman decoder estimated the actual hand movement with reasonable fidelity.

XI. CONCLUDING REMARKS

Substantial progress has been made in the last two decades in developing neural controllers for prosthetic limbs. The research in this area has progressed from computer models and animal experiments to experiments with human subjects. Assuming continued progress, it is

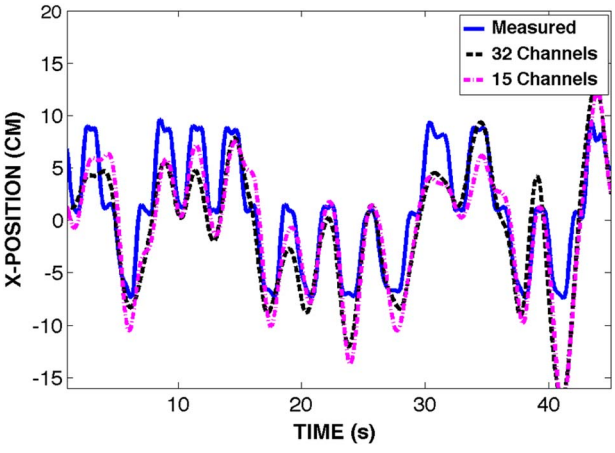

Fig. 11. *Measured and estimated hand movements from ECoG data. The decoder used a fifth-order nonlinear model with 32 and 15 channels and a five-sample memory. Only movements along the x-direction are shown, although the reconstruction errors along both axes were similar [141].*

reasonable to expect that low-cost and multiple DoF neural-controlled prosthetic hands that operate like natural hands will become available in the next decade. This paper reviewed two important mechanisms for recording control signals from the motor system to decode movement intents: action potentials from the PNS, and ECoG from the CNS. These two signals were selected because 1) they illustrate that it can be advantageous to record from different points along the motor control pathway; and 2) the methods described for these two signals may be easily adapted to other signals including CNS action potentials, LFP, EEG, ENG, and EMG.

PNS action potentials and ECoG signals both represent aspects of motor control; however, the specific content of these two signals can vary widely. For example, the PNS signal exclusively and directly corresponds to muscle contraction, so that the firing rate of a PNS neuron is likely to be highly correlated with movement about one or more joints. In contrast, ECoG is a population measure whose specificity depends upon the functional roles of the population members, and whose information content could represent a wider range of motor control elements spanning planning, initiation, and execution of more complex movements. These differences point toward tradeoffs to consider when evaluating signals for a particular neural prosthetic application. The most basic considerations are first, whether PNS signals exist, as in the case of an amputee, or do not exist, as in the case of a high-level spinal cord injury; and second, the level of risk that may be tolerated in the application. Although invasive surgery may not be acceptable in all cases, arm and hand functions consistently rank among the highest priorities to persons with motor disability and, in some populations, this need may warrant invasive procedures in return for restoration of capability [23]–[26]. Continued progress in fundamental scientific understanding of the PNS and CNS, electrode and prosthesis design, and machine learning technologies means that the tradeoffs inherent in selecting the appropriate signal for a neural prosthesis must be constantly reevaluated.

There are a number of areas that require additional work before the dream of prosthetic arms that act and feel like normal arms becomes feasible. As was seen from the results in Section X, when the desired number of DoFs of the movements increase, the decoder accuracy suffers. Additional work in improving the accuracy of multiple-DoF decoders is needed. However, it may also be the case that the decoders will always have a certain amount of residual error in their outputs that degrades controller performance. In this paper, we assumed that the decoder output is used directly to control the prosthetic limb. To overcome the problems associated with decoder errors, a better division of responsibilities between the decoder and the controller may be necessary. For example, it may be possible to develop a decoder that determines the goal for the prosthetic limb (for example, grasp an object) and allow the controller to design a control strategy to achieve the goal [150].

Visual and other sensory perceptions play a crucial role in how the nervous system controls human motor activity. It is also possible to integrate other body control elements, such as eye tracking, to provide goal or other information that could be used to improve the system. Although this paper did not discuss sensory feedback, work is ongoing in a number of laboratories to integrate sensory feedback with control of prosthetic limbs [13]–[15], [157].

Although there is no reason to believe that the nervous system behaves linearly, most neural decoders in the literature employ linear models. The results of our work as well as those of others indicate that substantial decoding improvements are possible through the use of nonlinear and possibly time-varying system models. Additional work to refine such techniques in neuroprosthetic control is still needed.

Almost all decoders in development now require training. Although training is not difficult to perform at the time of fitting the prosthesis, the system may change its characteristics over time. Practically all current techniques require retraining periodically. It is desirable to develop systems that eliminate the need for retraining, or at least decrease the frequency of retraining. This will require adaptive decoders that can learn and track the changes in neural system behavior over time. ■

Acknowledgment

The authors wish to thank Bradley Gregor, Heather Wark and David Page for their role in acquiring some of the data reported in this paper.

REFERENCES

[1] G. S. Dhillon, S. M. Lawrence, D. T. Hutchinson, and K. W. Horch, "Residual function in peripheral nerve stumps of amputees: Implications for neural control of artificial limbs," *J. Hand Surg. Amer.*, vol. 29, no. 4, pp. 605–615, 2004, discussion 616-8.

[2] G. S. Dhillon and K. W. Horch, "Direct neural sensory feedback and control of a prosthetic arm," *IEEE Trans. Neural Syst. Rehabil. Eng.*, vol. 13, no. 4, pp. 468–472, 2005.

[3] G. S. Dhillon, T. B. Kruger, J. S. Sandhu, and K. W. Horch, "Effects of short-term training on sensory and motor function in severed nerves of long-term human amputees," *J. Neurophysiol.*, vol. 93, no. 5, pp. 2625–2633, 2005.

[4] L. A. Miller *et al.*, "Control of a six degree of freedom prosthetic arm after targeted muscle reinnervation surgery," *Arch. Phys. Med. Rehabil.*, vol. 89, no. 11, pp. 2057–2065, 2008.

[5] S. Micera *et al.*, "On the control of a robot hand by extracting neural signals from the PNS: Preliminary results from a human implantation," in *Proc. Conf. IEEE Eng. Med. Biol. Soc.*, 2009, pp. 4586–4589.

[6] K. H. Polasek, H. A. Hoyen, M. W. Keith, R. F. Kirsch, and D. J. Tyler, "Stimulation stability and selectivity of chronically implanted multicontact nerve cuff electrodes in the human upper extremity," *IEEE Trans. Neural. Syst. Rehabil. Eng.*, vol. 17, no. 5, pp. 428–437, 2009.

[7] M. A. Schiefer, K. H. Polasek, R. J. Triolo, G. C. Pinault, and D. J. Tyler, "Intraoperative demonstration of selective stimulation of the common human femoral

nerve with a FINE," in *Proc. IEEE Conf. Eng. Med. Biol. Soc.*, 2009, pp. 610–613.

[8] S. Micera, J. Carpaneto, and S. Raspopovic, "Control of hand prostheses using peripheral information," *IEEE Rev. Biomed. Eng.*, vol. 3, pp. 48–68, 2010.

[9] S. Micera *et al.*, "Decoding information from neural signals recorded using intraneural electrodes: Toward the development of a neurocontrolled hand prosthesis," *Proc. IEEE*, vol. 98, no. 3, pp. 407–417, Mar. 2010.

[10] G. A. Clark, N. M. Ledbetter, D. J. Warren, and R. R. Harrison, "Recording sensory and motor information from peripheral nerves with Utah slanted electrode arrays," in *Proc. Annu. Int. Conf. IEEE Eng. Med. Biol. Soc.*, 2011, pp. 4641–4644.

[11] K. Horch, S. Meek, T. G. Taylor, and D. T. Hutchinson, "Object discrimination with an artificial hand using electrical stimulation of peripheral tactile and proprioceptive pathways with intrafascicular electrodes," *IEEE Trans. Neural Syst. Rehabil. Eng.*, vol. 19, no. 5, pp. 483–489, 2011.

[12] S. Micera *et al.*, "Decoding of grasping information from neural signals recorded using peripheral intrafascicular interfaces," *J. Neuroeng. Rehabil.*, vol. 8, p. 53, 2011.

[13] G. A. Clark *et al.*, "Using multiple high-count electrode arrays in human median and ulnar nerves to restore sensorimotor function after previous transradial amputation of the hand," in *Proc. 36th Annu. Int. Conf. IEEE Eng. Med. Biol. Soc.*, 2014, pp. 1977–1980.

[14] S. Raspopovic *et al.*, "Restoring natural sensory feedback in real-time bidirectional hand prostheses," *Sci. Transl. Med.*, vol. 6, no. 222, 2014, Art. ID 222ra19.

[15] D. W. Tan *et al.*, "A neural interface provides long-term stable natural touch perception," *Sci. Transl. Med.*, vol. 6, no. 257, 2014, Art. ID 257ra138.

[16] S. C. Jacobson, D. F. Knutti, R. T. Johnson, and H. H. Sears, "Development of the Utah artificial arm," *IEEE Trans. Biomed. Eng.*, vol. BME-29, no. 4, pp. 249–269, 1982.

[17] R. Branemark *et al.*, "A novel osseointegrated percutaneous prosthetic system for the treatment of patients with transfemoral amputation: A prospective study of 51 patients," *Bone Joint J.*, vol. 96-B, no. 1, pp. 106–113, 2014.

[18] T. A. Kuiken, G. A. Dumanian, R. D. Lipschutz, L. A. Miller, and K. A. Stubblefield, "The use of targeted muscle reinnervation for improved myoelectric prosthesis control in a bilateral shoulder disarticulation amputee," *Prosthet. Orthot. Int.*, vol. 28, no. 3, pp. 245–253, 2004.

[19] J. M. Burck, J. D. Bigelow, and S. D. Harshbarger, "Revolutionizing prosthetics: Systems engineering challenges and opportunities," *Johns Hopkins APL Tech. Dig.*, vol. 30, no. 3, pp. 186–197, 2011.

[20] M. S. Johannes *et al.*, "An overview of the developmental process for the modular prosthetic limb," *Johns Hopkins APL Tech. Dig.*, vol. 30, no. 3, pp. 207–216, 2011.

[21] L. Resnik, S. L. Klinger, and K. Etter, "The DEKA arm: Its features, functionality, and evolution during the veterans affairs study to optimize the DEKA arm," *Prosthet. Orthot. Int.*, vol. 38, no. 6, pp. 492–504, 2014.

[22] L. Resnik, S. L. Klinger, and K. Etter, "User and clinician perspectives on DEKA arm: Results of VA study to optimize DEKA arm," *J. Rehabil. Res. Dev.*, vol. 51, no. 1, pp. 27–38, 2014.

[23] C. H. Blabe *et al.*, "Assessment of brain-machine interfaces from the perspective of people with paralysis," *J. Neural Eng.*, vol. 12, no. 4, 2015, Art. ID 043002.

[24] K. D. Anderson, "Targeting recovery: Priorities of the spinal cord-injured population," *J. Neurotrauma*, vol. 21, no. 10, pp. 1371–1383, 2004.

[25] G. J. Snoek, M. J. IJzerman, H. J. Hermens, D. Maxwell, and F. Biering-Sorensen, "Survey of the needs of patients with spinal cord injury: Impact and priority for improvement in hand function in tetraplegics," *Spinal Cord*, vol. 42, no. 9, pp. 526–532, 2004.

[26] J. L. Collinger *et al.*, "Functional priorities, assistive technology, and brain-computer interfaces after spinal cord injury," *J. Rehabil. Res. Develop.*, vol. 50, no. 2, p. 145, 2013.

[27] P. R. Kennedy, R. A. Bakay, M. M. Moore, K. Adams, and J. Goldwaithe, "Direct control of a computer from the human central nervous system," *IEEE Trans. Rehabil. Eng.*, vol. 8, pp. 198–202, 2000.

[28] P. G. Patil, J. M. Carmena, M. A. Nicolelis, and D. A. Turner, "Ensemble recordings of human subcortical neurons as a source of motor control signals for a brain-machine interface," *Neurosurgery*, vol. 55, no. 1, pp. 27–35, 2004, discussion 35-8.

[29] L. R. Hochberg *et al.*, "Neuronal ensemble control of prosthetic devices by a human with tetraplegia," *Nature*, vol. 442, no. 7099, pp. 164–171, 2006.

[30] T. A. Kuiken *et al.*, "Targeted muscle reinnervation for real-time myoelectric control of multifunction artificial arms," *JAMA*, vol. 301, no. 6, pp. 619–628, 2009.

[31] D. Sussillo *et al.*, "A recurrent neural network for closed-loop intracortical brain-machine interface decoders," *J. Neural Eng.*, vol. 9, 2012, Art. ID 026027.

[32] M. Ortiz-Catalan, R. Brånemark, B. Håkansson, and J. Delbeke, "On the viability of implantable electrodes for the natural control of artificial limbs: Review and discussion," *Biomed. Eng. Online*, vol. 11, 2012.

[33] J. L. Collinger *et al.*, "High-performance neuroprosthetic control by an individual with tetraplegia," *Lancet*, vol. 381, no. 9866, pp. 557–564, 2013.

[34] D. U. Silverthorn, B. R. Johnson, W. C. Ober, C. W. Garrison, and A. C. Silverthorn, *Human Physiology: An Integrated Approach*. Boston, MA, USA: Pearson Education, 2013.

[35] R. M. Berne, M. N. Levy, and B. M. Koeppen, *Physiology*. St. Louis, MO, USA: Mosby, 2004.

[36] E. R. Kandel, *Principles of Neural Science*, New York, NY, USA: McGraw-Hill, 2013.

[37] G. Buzsaki, C. A. Anastassiou, and C. Koch, "The origin of extracellular fields and currents—EEG, ECoG, LFP and spikes," *Nature Rev. Neurosci.*, vol. 13, no. 6, pp. 407–420, 2012.

[38] M. Weinrich and S. P. Wise, "The premotor cortex of the monkey," *Neuroscience*, vol. 2, pp. 1329–1345, 1982.

[39] H. Mushiake, M. Inase, and J. Tanji, "Neuronal activity in the primate premotor cortex during visually guided and internally determined sequential movements," *J. Neurophysiol.*, vol. 66, pp. 705–718, 1991.

[40] E. V. Evarts, "Relation of pyramidal tract activity to force exerted during voluntary movement," *J. Neurophysiol.*, vol. 31, no. 1, pp. 14–27, Jan. 1968.

[41] E. E. Fetz and P. D. Cheney, "Postspike facilitation of forelimb muscle activity by primate corticomotoneuronal cells," *J. Neurophysiol.*, vol. 44, no. 4, pp. 751–772, Oct. 1980.

[42] J. F. Kalaska, D. A. Cohen, M. L. Hyde, and M. Prud'homme, "A comparison of movement direction-related versus load direction-related activity in primate motor cortex, using a two-dimensional reaching task," *J. Neurosci.*, vol. 9, no. 6, pp. 2080–2102, Jun. 1989.

[43] A. Georgopoulos, J. Kalaska, R. Caminiti, and J. Massey, "On the relations between the direction of two-dimensional arm movements and cell discharge in primate motor cortex," *J. Neurosci.*, vol. 2, no. 11, pp. 1527–1537, 1982.

[44] D. W. Moran and A. B. Schwartz, "Motor cortical representation of speed and direction during reaching," *J. Neurophysiol.*, vol. 82, no. 5, pp. 2676–2692, Nov. 1999.

[45] E. Todorov, "Direct cortical control of muscle activation in voluntary arm movements: A model," *Nature Neurosci.*, vol. 3, no. 4, pp. 391–398, Apr. 2000.

[46] G. Buzsaki and A. Draguhn, "Neuronal oscillations in cortical networks," *Science*, vol. 304, no. 5679, pp. 1926–1929, 2004.

[47] M. S. Lewicki, "A review of methods for spike sorting: The detection and classification of neural action potentials," *Network*, vol. 9, no. 4, pp. R53–R78, 1998.

[48] G. Santhanam, S. I. Ryu, B. M. Yu, A. Afshar, and K. V. Shenoy, "A high-performance brain-computer interface," *Nature*, vol. 442, no. 7099, pp. 195–198, 2006.

[49] E. Stark and M. Abeles, "Predicting movement from multiunit activity," *J. Neurosci.*, vol. 27, no. 31, pp. 8387–8394, 2007.

[50] G. W. Fraser, S. M. Chase, A. Whitford, and A. B. Schwartz, "Control of a brain-computer interface without spike sorting," *J. Neural Eng.*, vol. 6, no. 5, 2009, Art. ID 055004.

[51] C. A. Chestek *et al.*, "Long-term stability of neural prosthetic control signals from silicon cortical arrays in rhesus macaque motor cortex," *J. Neural Eng.*, vol. 8, no. 4, 2011, Art. ID 045005.

[52] S. Todorova, P. Sadtler, A. Batista, S. Chase, and V. Ventura, "To sort or not to sort: The impact of spike-sorting on neural decoding performance," *J. Neural Eng.*, vol. 11, no. 5, 2014, Art. ID 056005.

[53] R. A. Andersen, S. Musallam, and B. Pesaran, "Selecting the signals for a brain-machine interface," *Curr. Opin. Neurobiol.*, vol. 14, no. 6, pp. 720–726, 2004.

[54] R. D. Flint, Z. A. Wright, M. R. Scheid, and M. W. Slutzky, "Long term, stable brain machine interface performance using local field potentials and multiunit spikes," *J. Neural Eng.*, vol. 10, no. 5, 2013, Art. ID 056005.

[55] D. Wang *et al.*, "Long-term decoding stability of local field potentials from silicon arrays in primate motor cortex

during a 2D center out task," *J. Neural Eng.*, vol. 11, no. 3, 2014, Art. ID 036009.

[56] A. K. Bansal, C. E. Vargas-Irwin, W. Truccolo, and J. P. Donoghue, "Relationships among low-frequency local field potentials, spiking activity, and three-dimensional reach and grasp kinematics in primary motor and ventral premotor cortices," *J. Neurophys.*, vol. 105, no. 4, pp. 1603–1619, 2011.

[57] J. Zhuang, W. Truccolo, C. Vargas-Irwin, and J. P. Donoghue, "Decoding 3-D reach and grasp kinematics from high-frequency local field potentials in primate primary motor cortex," *IEEE Trans. Biomed. Eng.*, vol. 57, no. 7, pp. 1774–1784, 2010.

[58] E. J. Hwang and R. A. Andersen, "Brain control of movement execution onset using local field potentials in posterior parietal cortex," *J. Neurosci.*, vol. 29, no. 45, pp. 14 363–14 370, 2009.

[59] E. J. Hwang and R. A. Andersen, "Spiking and LFP activity in PRR during symbolically instructed reaches," *J. Neurophys.*, vol. 107, no. 3, pp. 836–849, 2012.

[60] E. J. Hwang and R. A. Andersen, "The utility of multichannel local field potentials for brain-machine interfaces," *J. Neural Eng.*, vol. 10, no. 4, 2013, Art. ID 046005.

[61] K. So, S. Dangi, A. L. Orsborn, M. C. Gastpar, and J. M. Carmena, "Subject-specific modulation of local field potential spectral power during brain-machine interface control in primates," *J. Neural Eng.*, vol. 11, no. 2, 2014, Art. ID 026002.

[62] D. A. Heldman, W. Wang, S. S. Chan, and D. W. Moran, "Local field potential spectral tuning in motor cortex during reaching," *IEEE Trans. Neural Syst. Rehabil. Eng.*, vol. 14, no. 2, pp. 180–183, 2006.

[63] J. P. Donoghue, J. N. Sanes, N. G. Hatsopoulos, and G. Gaál, "Neural discharge and local field potential oscillations in primate motor cortex during voluntary movements," *J. Neurophys.*, vol. 79, no. 1, pp. 159–173, 1998.

[64] H. Scherberger, M. R. Jarvis, and R. A. Andersen, "Cortical local field potential encodes movement intentions in the posterior parietal cortex," *Neuron*, vol. 46, no. 2, pp. 347–354, 2005.

[65] C. Mehring *et al.*, "Inference of hand movements from local field potentials in monkey motor cortex," *Nature Neurosci.*, vol. 6, no. 12, pp. 1253–1254, 2003.

[66] N. F. Ince *et al.*, "High accuracy decoding of movement target direction in non-human primates based on common spatial patterns of local field potentials," *PLoS One*, vol. 5, no. 12, 2010, e14384.

[67] J. Rickert *et al.*, "Encoding of movement direction in different frequency ranges of motor cortical local field potentials," *J. Neurosci.*, vol. 25, no. 39, pp. 8815–8824, 2005.

[68] S. S. Kellis, P. A. House, K. E. Thomson, R. Brown, and B. Greger, "Human neocortical electrical activity recorded on nonpenetrating microwire arrays: Applicability for neuroprostheses," *Neurosurgery Focus*, vol. 27, no. 1, p. E9, 2009.

[69] S. Kellis *et al.*, "Decoding spoken words using local field potentials recorded from the cortical surface," *J. Neural Eng.*, vol. 7, no. 5, 2010, Art. ID 056007.

[70] D. T. Bundy *et al.*, "Characterization of the effects of the human dura on macro-and micro-electrocorticographic recordings," *J. Neural Eng.*, vol. 11, no. 1, 2014, Art. ID 016006.

[71] D.-H. Kim *et al.*, "Dissolvable films of silk fibroin for ultrathin conformal bio-integrated electronics," *Nature Mater.*, vol. 9, no. 6, pp. 511–517, 2010.

[72] W. Wang *et al.*, "Human motor cortical activity recorded with micro-ECoG electrodes, during individual finger movements," in *Proc. Conf. IEEE Eng. Med. Biol. Soc.*, Sep. 3–6, 2009, pp. 586–589.

[73] N. R. Anderson, T. Blakely, G. Schalk, E. C. Leuthardt, and D. W. Moran, "Electrocorticographic (ECoG) correlates of human arm movements," *Exp. Brain Res.*, vol. 223, no. 1, pp. 1–10, 2012.

[74] C. A. Chestek *et al.*, "Hand posture classification using electrocorticography signals in the gamma band over human sensorimotor brain areas," *J. Neural Eng.*, vol. 10, no. 2, 2013 Art. ID 026002.

[75] J. L. Collinger *et al.*, "Motor-related brain activity during action observation: A neural substrate for electrocorticographic brain-computer interfaces after spinal cord injury," *Front. Integr. Neurosci.*, vol. 8, 2014.

[76] S. Kellis *et al.*, "Decoding hand trajectories from micro-electrocorticography in human patients," in *Proc. Annu. Int. Conf. IEEE Eng. Med. Biol. Soc.*, 2012, pp. 4091–4094.

[77] E. C. Leuthardt, Z. Freudenberg, D. Bundy, and J. Roland, "Microscale recording from human motor cortex: Implications for minimally invasive electrocorticographic brain-computer interfaces," *Neurosurgical Focus*, vol. 27, no. 1, p. E10, 2009.

[78] K. J. Miller *et al.*, "Spectral changes in cortical surface potentials during motor movement," *J. Neurosci.*, vol. 27, no. 9, pp. 2424–2432, 2007.

[79] G. Schalk *et al.*, "Decoding two-dimensional movement trajectories using electrocorticographic signals in humans," *J. Neural Eng.*, vol. 4, no. 3, p. 264, 2007.

[80] Z. Wang *et al.*, "Decoding onset and direction of movements using electrocorticographic (ECoG) signals in humans," *Front. Neuroeng.*, vol. 5, 2012.

[81] W. Wang *et al.*, "An electrocorticographic brain interface in an individual with tetraplegia," *PloS One*, vol. 8, no. 2, 2013, Art. ID e55344.

[82] M. Hansen, M. Haugland, T. Sinkjaer, and N. Donaldson, "Real time foot drop correction using machine learning and natural sensors," *Neuromodulation*, vol. 5, no. 1, pp. 41–53, 2002.

[83] D. Farina and A. Holobar, "Characterization of human muscle activity from body surface recordings," *Proc. IEEE*, vol. 104, no. 2, Feb. 2016, DOI: 10.1109/JPROC.2015.2498665.

[84] C. T. Nordhausen, P. J. Rousche, and R. A. Normann, "Optimizing recording capabilities of the Utah intracortical electrode array," *Brain Res.*, vol. 637, no. 1–2, pp. 27–36, 1994.

[85] P. K. Campbell, K. E. Jones, R. J. Huber, K. W. Horch and R. A. Normann, "A silicon-based, three-dimensional neural interface: Manufacturing processes for an intracortical electrode array," *IEEE Trans. Biomed. Eng.*, vol. 38, pp. 758–768, 1991.

[86] A. Starr, K. D. Wise, and J. Csongradi, "An evaluation of photoengraved microelectrodes for extracellular single-unit recording," *IEEE Trans. Biomed. Eng.*, vol. 20, pp. 291–293, 1973.

[87] A. C. Hoogerwerf and K. D. Wise, "A three-dimensional microelectrode array for chronic neural recording," *IEEE Trans. Biomed. Eng.*, vol. 41, pp. 1136–1146, 1994.

[88] D. J. Weber, R. Friesen, and L. E. Miller, "Interfacing the somatosensory system to restore touch and proprioception: Essential considerations," *J. Mot. Behav.*, vol. 44, no. 6, pp. 403–418, 2012.

[89] D. J. Tyler and D. M. Durand, "Chronic response of the rat sciatic nerve to the flat interface nerve electrode," *Ann. Biomed. Eng.*, vol. 31, pp. 633–642, 2003.

[90] D. Calvetti, B. Wodlinger, D. M. Durand, and E. Somersalo, "Hierarchical beamformer and cross-talk reduction in electroneurography," *J. Neural Eng.*, vol. 8, 2011, Art. ID 056002.

[91] Y. Tang, B. Wodlinger, and D. M. Durand, "Bayesian spatial filters for source signal extraction: A study in the peripheral nerve," *IEEE Trans. Neural Syst. Rehabil. Eng.*, vol. 22, pp. 302–311, 2014.

[92] B. Wodlinger and D. M. Durand, "Localization and recovery of peripheral neural sources with beamforming algorithms," *IEEE Trans. Neural Syst. Rehabil. Eng.*, vol. 17, no. 5, pp. 461–468, 2009.

[93] M. S. Malagodi, K. W. Horch, and A. A. Schoenberg, "An intrafascicular electrode for recording of action potentials in peripheral nerves," *Ann. Biomed. Eng.*, vol. 17, pp. 397–410, 1989.

[94] S. Snow, S. C. Jacobsen, D. L. Wells, and K. W. Horch, "Microfabricated cylindrical multielectrodes for neural stimulation," *IEEE Trans. Biomed.Eng.*, vol. 53, no. 2, pp. 320–326, 2006.

[95] T. Boretius *et al.*, "A transverse intrafascicular multichannel electrode (TIME) to interface with the peripheral nerve," *Biosens. Bioelectr.*, vol. 26, no. 1, pp. 62–69, 2010.

[96] A. Branner, R. B. Stein, and R. A. Normann, "Selective stimulation of cat sciatic nerve using an array of varying-length microelectrodes," *J. Neurophysiol.*, vol. 85, pp. 1585–1594, 2001.

[97] S. Kellis, B. Greger, S. Hanrahan, P. House, and R. Brown, "Platinum microwire for subdural electrocorticography over human neocortex: Millimeter-scale spatiotemporal dynamics," in *Proc. Annu. Conf. IEEE Eng. Med. Biol. Soc.*, 2011, pp. 4761–4765.

[98] T. H. Bullock *et al.*, "EEG coherence has structure in the millimeter domain: Subdural and hippocampal recordings from epileptic patients," *Electroenceph. Clin. Neurophys.*, vol. 95, no. 3, pp. 161–177, 1995.

[99] A. Flinker, E. F. Chang, N. M. Barbaro, M. S. Berger, and R. T. Knight, "Sub-centimeter language organization in the human temporal lobe," *Brain Lang.*, vol. 117, no. 3, pp. 103–109, 2011.

[100] J. Viventi *et al.*, "Flexible, foldable, actively multiplexed, high-density electrode array for mapping brain activity *in vivo*," *Nature Neurosci.*, vol. 14, no. 12, pp. 1599–1605, 2011.

[101] J. D. Simeral, S. P. Kim, M. J. Black, J. P. Donoghue, and L. R. Hochberg, "Neural control of cursor trajectory and click by a human with tetraplegia 1000 days after implant of an intracortical microelectrode array," *J. Neural Eng.*, vol. 8, no. 2, 2011, Art. ID 025027.

[102] G. W. Fraser and A. B. Schwartz, "Recording from the same neurons chronically in motor

cortex," *J. Neurophysiol.*, vol. 107, no. 7, pp. 1970–1978, 2012.

[103] P. Takmakov *et al.*, "Rapid evaluation of the durability of cortical neural implants using accelerated aging with reactive oxygen species," *J. Neural Eng.*, vol. 12, no. 2, 2015, Art. ID 026003.

[104] S. M. Lawrence, J. O. Larsen, K. W. Horch, R. Riso, and T. Sinkjaer, "Long-term biocompatibility of implanted polymer-based intrafascicular electrodes," *J. Biomed. Mater. Res.*, vol. 63, no. 5, pp. 501–506, 2002.

[105] A. K. Bansal, W. Truccolo, C. E. Vargas-Irwin, and J. P. Donoghue, "Decoding 3D reach and grasp from hybrid signals in motor and premotor cortices: Spikes, multiunit activity, and local field potentials," *J. Neurophys.*, vol. 107, no. 5, pp. 1337–1355, 2012.

[106] Z. C. Chao, Y. Nagasaka, and N. Fujii, "Long-term asynchronous decoding of arm motion using electrocorticographic signals in monkeys," *Front. Neuroeng.*, vol. 3, 2010.

[107] C. Henle *et al.*, "First long term *in vivo* study on subdurally implanted micro-ECoG electrodes, manufactured with a novel laser technology," *Biomed. Microdevices*, vol. 13, no. 1, pp. 59–68, 2011.

[108] M. Zardoshti-Kermani, B. C. Wheeler, K. Badie, and R. M. Hashemi, "EMG feature evaluation for movement control of upper extremity prostheses," *IEEE Trans. Rehabil. Eng.*, vol. 3, no. 4, pp. 324–333, 1995.

[109] K. Englehart, B. Hudgins, P. A. Parker, and M. Stevenson, "Classification of the myoelectric signal using time-frequency based representations," *Med. Eng. Phys.*, vol. 21, no. 6/7, pp. 431–438, 1999.

[110] J. J. Baker, E. Scheme, K. Englehart, D. T. Hutchinson, and B. Greger, "Continuous detection and decoding of dexterous finger flexions with implantable myoelectric sensors," *IEEE Trans. Neural Syst. Rehabil. Eng.*, vol. 18, no. 4, pp. 424–432, 2010.

[111] A. Fougner, E. Scheme, A. D. C. Chan, K. Englehart, and Ã. Stavdahl, "Resolving the limb position effect in myoelectric pattern recognition," *IEEE Trans. Neural Syst. Rehabil. Eng.*, vol. 19, no. 6, pp. 644–651, 2011.

[112] A. J. Young, L. J. Hargrove, and T. A. Kuiken, "Improving myoelectric pattern recognition robustness to electrode shift by changing interelectrode distance and electrode configuration," *IEEE Trans. Biomed. Eng.*, vol. 59, no. 3, pp. 645–652, 2012.

[113] L. Liu, P. Liu, E. A. Clancy, E. Scheme, and K. B. Englehart, "Electromyogram whitening for improved classification accuracy in upper limb prosthesis control," *IEEE Trans. Neural Syst. Rehabil. Eng.*, vol. 21, no. 5, pp. 767–774, 2013.

[114] E. Scheme and K. B. Englehart, "Validation of a selective ensemble-based classification scheme for myoelectric control using a three-dimensional Fitts' law test," *IEEE Trans. Neural Syst. Rehabil. Eng.*, vol. 21, no. 4, pp. 616–623, 2013.

[115] E. J. Scheme, B. S. Hudgins, and K. B. Englehart, "Confidence-based rejection for improved pattern recognition myoelectric control," *IEEE Trans. Biomed. Eng.*, vol. 60, no. 6, pp. 1563–1570, 2013.

[116] P. Shenoy, K. J. Miller, J. G. Ojemann, and R. P. Rao, "Finger movement classification for an electrocorticographic BCI," in *Proc. 3rd Int. IEEE/EMBS Conf. Neural Eng.*, 2007, pp. 192–195.

[117] P. Shenoy, K. J. Miller, J. G. Ojemann, and R. P. Rao, "Generalized features for electrocorticographic BCIs," *IEEE Trans. Biomed. Eng.*, vol. 55, no. 1, pp. 273–280, 2008.

[118] M. Bleichner *et al.*, "Give me a sign: Decoding four complex hand gestures based on high-density ecog," *Brain Struct. Funct.*, pp. 1–14, 2014.

[119] T. Wissel *et al.*, "Hidden markov model and support vector machine based decoding of finger movements using electrocorticography," *J. Neural Eng.*, vol. 10, no. 5, 2013, Art. ID 056020.

[120] P. M. Rossini *et al.*, "Double nerve intraneural interface implant on a human amputee for robotic hand control," *Clin. Neurophysiol.*, vol. 121, no. 5, pp. 777–783, 2010.

[121] G. Di Pino *et al.*, "Overview of the implant of intraneural multielectrodes in human for controlling a 5-fingered hand prosthesis, delivering sensorial feedback and producing rehabilitative neuroplasticity," in *Proc. IEEE BioRob*, 2012, pp. 1831–1836.

[122] E. C. Leuthardt, G. Schalk, J. R. Wolpaw, J. G. Ojemann, and D. W. Moran, "A brain-computer interface using electrocorticographic signals in humans," *J. Neural Eng.*, vol. 1, no. 2, pp. 63–71, 2004.

[123] E. C. Leuthardt, K. J. Miller, G. Schalk, R. P. Rao, and J. G. Ojemann, "Electrocorticography-based brain computer interface-the Seattle experience," *IEEE Trans. Neural Syst. Rehabil. Eng.*, vol. 14, no. 2, pp. 194–198, 2006.

[124] J. Hammer *et al.*, "The role of ECoG magnitude and phase in decoding position, velocity, and acceleration during continuous motor behavior," *Front. Neurosci.*, vol. 7, 2013.

[125] Y. Nakanishi *et al.*, "Prediction of three-dimensional arm trajectories based on ECoG signals recorded from human sensorimotor cortex," *PloS One*, vol. 8, no. 8, 2013, Art. ID e72085.

[126] K. J. Miller *et al.*, "Cortical activity during motor execution, motor imagery, and imagery-based online feedback," *Proc. Nat. Acad. Sci.*, vol. 107, no. 9, pp. 4430–4435, 2010.

[127] R. Flamary and A. Rakotomamonjy, "Decoding finger movements from ECoG signals using switching linear models," *Front. Neurosci.*, vol. 6, 2012.

[128] S. Acharya, M. S. Fifer, H. L. Benz, N. E. Crone, and N. V. Thakor, "Electrocorticographic amplitude predicts finger positions during slow grasping motions of the hand," *J. Neural Eng.*, vol. 7, no. 4, 2010, Art. ID 046002.

[129] N. Liang and L. Bougrain, "Decoding finger flexion from band-specific ECoG signals in humans," *Front. Neurosci.*, vol. 6, 2012.

[130] K. Warwick *et al.*, "The application of implant technology for cybernetic systems," *Arch. Neurol.*, vol. 60, no. 10, pp. 1369–1373, 2003.

[131] F. F. Offner, "The EEG as potential mapping: The value of the average monopolar reference," *Electroencephal. Clin. Neurophys.*, vol. 2, pp. 213–214, 1950.

[132] K. A. Ludwig *et al.*, "Using a common average reference to improve cortical neuron recordings from microelectrode arrays," *J. Neurophy.*, vol. 101, pp. 1679–1689, 2009.

[133] M. S. Lemos and B. Fisch, "The weighted average reference montage," *Electroencephal. Clin. Neurophys.*, vol. 79, no. 5, pp. 361–370, 1991.

[134] B. Hjorth, "An on-line transformation of EEG scalp potentials into orthogonal source derivations," *Electroencephal. Clin. Neurophys.*, vol. 39, no. 5, pp. 526–530, 1975.

[135] C. Tandonnet and B. B, "EEG traces by surface Laplacian estimation: Comparison between local and global methods," *Clin. Neurophys.*, vol. 116, no. 1, pp. 18–24, 2005.

[136] H. Bokil, P. Andrews, J. E. Kulkarni, S. Mehta, and P. P. Mitra, "Chronux: A platform for analyzing neural signals," *J. Neurosci. Meth.*, vol. 192, no. 1, pp. 146–151, 2010.

[137] B. Widrow *et al.*, "Adaptive noise cancelling: Principles and applications," *Proc. IEEE*, vol. 63, no. 12, pp. 1692–1716, Dec. 1975.

[138] R. T. Canolty and R. T. Knight, "The functional role of cross-frequency coupling," *Trends Cogn. Sci.*, vol. 14, no. 11, pp. 506–515, 2010.

[139] W. J. Freeman, M. D. Holmes, G. A. West, and S. Vanhatalo, "Fine spatiotemporal structure of phase in human intracranial EEG," *Clin. Neurophysiol.*, vol. 117, no. 6, pp. 1228–1243, 2006.

[140] R. Wahnoun, J. He and S. I. H. Tillery, "Selection and parameterization of cortical neurons for neuroprosthetic control," *J. Neural Eng.*, vol. 3, no. 2, p. 162, 2006.

[141] H. Dantas, S. Kellis, V. Mathews, and B. Greger, "Neural decoding using a nonlinear generative model for brain-computer interface," in *Proc. IEEE Int. Conf. Acoust. Speech Signal Process.*, 2014, pp. 4683–4687.

[142] I. Jolliffe, *Principal Component Analysis*, New York, NY, USA: Wiley, 2002.

[143] A. Hyvärinen, J. Karhunen, and E. Oja, *Independent Component Analysis*. New York, NY, USA: Wiley, 2004, vol. 46.

[144] A. Bashashati, M. Fatourechi, R. K. Ward, and G. E. Birch, "A survey of signal processing algorithms in brain-computer interfaces based on electrical brain signals," *J. Neural Eng.*, vol. 4, no. 2, p. R32, 2007.

[145] W. Wu, Y. Gao, E. Bienenstock, J. P. Donoghue, and M. J. Black, "Bayesian population decoding of motor cortical activity using a Kalman filter," *Neural Comput.*, vol. 18, no. 1, pp. 80–118, 2006.

[146] S. Kim, J. Simeral, L. Hochberg, J. Donoghue, and M. Black, "Neural control of computer cursor velocity by decoding motor cortical spiking activity in humans with tetraplegia," *J. Neural Eng.*, vol. 5, pp. 455–476, 2008.

[147] V. Gilja, *et al.*, "A high-performance neural prosthesis enabled by control algorithm design," *Nature Neurosci.*, vol. 15, no. 12, p. 1752–1757, 2012.

[148] S. Gowda, *et al.*, "Designing dynamical properties of brain-machine interfaces to optimize task-specific performance," *IEEE Trans. Neural Syst. Rehabil. Eng.*, vol. 22, no. 5, p. 911–920, 2014.

[149] A. R. C. Paiva, I. Park, and J. Principe, "A reproducing kernel Hilbert space framework for spike train signal processing," *Neural Comput.*, vol. 21, no. 2, pp. 424–449, 2009.

[150] G. H. Mulliken, S. Musallam, and R. A. Andersen, "Decoding trajectories from posterior parietal cortex ensembles," *J. Neurosci.*, vol. 28, pp. 12913–12926, 2008.

[151] S. Dangi *et al.*, "Continuous closed-loop decoder adaptation with a recursive maximum likelihood algorithm allows for rapid performance acquisition in brain-machine interfaces," *Neural Comput.*, vol. 12, pp. 1–29, 2014.

[152] Y. G. Y. Gao, M. J. Black, E. Bienenstock, W. Wu, and J. P. Donoghue, "A quantitative comparison of linear and non-linear models of motor cortical activity for the encoding and decoding of arm motions," in *Proc. IEEE EMBS Conf. Neural Eng.*, 2003, pp. 189–192.

[153] S.-P. Kim *et al.*, "A comparison of optimal MIMO linear and nonlinear models for brain-machine interfaces," *J. Neural Eng.*, vol. 3, pp. 145–161, 2006.

[154] B. Yu, J. Cunningham, K. Shenoy, and M. Sahani, "Neural decoding of movements: From linear to nonlinear trajectory models," in *Neural Information Processing*. Berlin, Germany: Springer-Verlag, 2008, vol. 4984, pp. 586–595.

[155] Z. Li, J. O'Doherty, and T. Hanson, "Unscented Kalman filter for brain-machine interfaces," *PloS One*, vol. 4, no. 7, 2009, Art. ID e6243.

[156] R. Davoodi, C. Urata, M. Hauschild, M. Khachani, and G. Loeb, "Model-based development of neural prostheses for movement," *IEEE Trans. Biomed. Eng.*, vol. 54, no. 11, pp. 1909–1918, 2007.

[157] G. A. Tabot *et al.*, "Restoring the sense of touch with a prosthetic hand through a brain interface," *Proc. Nat. Acad. Sci. USA*, vol. 110, no. 45, pp. 18279–18284, 2013.

ABOUT THE AUTHORS

David J. Warren (Senior Member, IEEE) received the B.S. degree in electrical engineering from Washington State University, Pullman, WA, USA, in 1979, the M.S. degree in electrical engineering from the University of Washington, Seattle, WA, USA, in 1982, and the Ph.D. degree in bioengineering from the University of Utah, Salt Lake City, UT, USA, in 2006.

Currently, he is the Research Director for the Center for Neural Engineering and a Research Assistant Professor in the Department of Bioengineering, University of Utah. His research focuses on the decoding of afferent and encoding of efferent neuronal signals in the peripheral nervous system for use with neuroprostheses to restore sensory and motor function after spinal cord injury or limb loss.

Spencer Kellis (Member, IEEE) was born in St. Louis, MO, USA, in 1980. He received the B.S. degree in electrical engineering from Brigham Young University, Provo, UT, USA, in 2006 and the M.S. and Ph.D. degrees in electrical engineering from the University of Utah, Salt Lake City, UT, USA, in 2009 and 2012, respectively.

In 2012, he was appointed a Postdoctoral Scholar at the California Institute of Technology, Pasadena, CA, USA, in the Division of Biology and Biological Engineering. Previously, he worked as a summer intern at Intel Corporation, Folsom, CA, USA and Blackrock Microsystems, Salt Lake City, UT, USA. His current research interests include signal processing and algorithms for neural interfaces, applications of neural engineering to medical care and rehabilitation, and low-power VLSI for implantable microsystems.

Dr. Kellis is a member of the Society for Neuroscience (SfN).

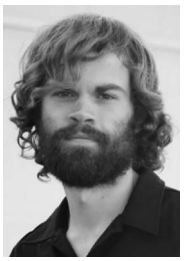

Jacob G. Nieveen was born in 1988. He received the M.S. degree in electrical engineering from Utah State University, Logan, UT, USA, in 2013. He is currently working toward the Ph.D. degree in the Department of Electrical and Computer Engineering at the University of Utah, Salt Lake City, UT, USA.

Prior to this, he was a DSP algorithms engineer at Wavetronix, a company focused in radar and other technologies for intelligent transportation systems.

Suzanne M. Wendelken received the B.A. degree in engineering physics and the M.S. degree in biomedical engineering from Dartmouth College, Hanover, NH, USA. She is currently working toward the Ph.D. degree in the M.D.-Ph.D. program at the University of Utah, Salt Lake City, UT, USA.

Her current research focus is on restoring sensory and motor function to upper limb amputees using implanted neural or myoelectric devices or surface electrodes.

Henrique Dantas received the Engineer degree and the M.Sc. degree in computer science from Universidade Federal de Pernambuco, Brazil, in 2013 and 2015, respectively. Currently, he is working toward the Ph.D. degree in electrical and computer engineering at Oregon State University, Corvallis, OR, USA.

He is focusing his studies on the biomedical engineering and machine learning fields.

Tyler S. Davis received the M.D. and Ph.D. degrees from the University of Utah, Salt Lake City, UT, USA, in 2007 and 2013, respectively.

He is currently a Postdoctoral Fellow in the Department of Neurosurgery, University of Utah. His research interests include the development of clinically viable neural interface systems for a broad range of applications including prosthetics and the treatment of epilepsy.

Douglas T. Hutchinson specializes in hand and microvascular surgery, and currently serves as the Hand Fellowship Director at the University of Utah, Salt Lake City, UT, USA and Chief of Hand Surgery at Primary Childrens Medical Center, the Veterans Affairs Medical Center, and Shriners Intermountain Hospital. He also holds an adjunct appointment in the Departments of Bioengineering and Physical Therapy. His research interests include neuroprosthetic applications for amputees, randomized, prospective clinical studies, and congenital deformities. He trained at Jefferson Medical College in Philadelphia, PA, USA, completed residency at Thomas Jefferson University Hospital in Philadelphia, PA, USA, and fellowship at the Raymond M. Curtis Hand Center in Baltimore, MD, USA.

Dr. Hutchinson is board certified in orthopaedics, and holds the Certificate of Added Qualification (CAQ) in Hand Surgery. His professional memberships include the American Academy of Orthopaedic Surgeons, the American Society for Surgery of the Hand, Orthopaedics Overseas, and the International Wrist Investigators Workshop.

Richard A. Normann is a Distinguished Emeritus Professor of Bioengineering and Ophthalmology at the University of Utah, Salt Lake City, UT, USA, where he conducts research on sensory encoding and information processing by neural ensembles in the vertebrate central and peripheral nervous systems. He is the inventor of the Utah Electrode Array technologies and other high-electrode-count microelectrode arrays that can be used for basic and applied research in emerging field of neuroprosthetics. His current research interests are the cortically based restoration of vision in those with profound blindness, and peripheral nerve interventions for the restoration of stance and for the control of prosthetic limbs and bladder control in those who have lost these functions.

Gregory A. Clark (Member, IEEE) received the Ph.D. degree from the University of California, Irvine, CA, USA.

He is an Associate Professor in the Department of Bioengineering, University of Utah, Salt Lake City, UT, USA. His research focuses primarily on using interfaces to the peripheral nervous system to restore sensorimotor function after limb amputation or spinal cord injury.

V. John Mathews (Fellow, IEEE) received the B.E. degree (honors) in electronics and communication engineering from the University of Madras, Madras, India, in 1980 and the M.S. and Ph.D. degrees in electrical and computer engineering from the University of Iowa, Iowa City, IA, USA, in 1981 and 1984, respectively.

He joined the Oregon State University, Corvallis, OR, USA, in 2015 as Professor and Head of the School of Electrical Engineering and Computer Science. He was at the University of Utah, Salt Lake City, UT, USA, from 1985 to 2015 where he was most recently Professor of Electrical and Computer Engineering. He served as the Chairman of the Department from 1999 to 2003. His research interests include adaptive and nonlinear systems, and applications of signal processing techniques in communication, audio, aerospace, neural engineering and biomedicine. He is the author of the book *Polynomial Signal Processing* (New York, NY, USA: Wiley, 2000). He has published more than 150 technical papers, and is the inventor on seven patents.

Dr. Mathews served as the Vice President-Finance of the IEEE Signal Processing Society from 2003 to 2005, and as Vice President-Conferences of the Society from 2011 to 2013. He has served on the publications board and the conference board of the Signal Processing Society. He has served on the editorial boards of the IEEE Transactions on Signal Processing, IEEE Signal Processing Letters, the IEEE Signal Processing Magazine, and the IEEE Journal of Selected Topics in Signal Processing. He has served on the organization committees of several international technical conferences, including as General Chairman of the 2001 IEEE International Conference on Acoustics, Speech and Signal Processing (ICASSP). He is a recipient of the 2008–2009 Distinguished Alumni Award from the National Institute of Technology, Tiruchirappalli, India; IEEE Utah Section's Engineer of the Year Award in 2001; and the Utah Engineers Council's Engineer of the Year Award in 2011. He was a Distinguished Lecturer of the IEEE Signal Processing Society for 2013 and 2014, and is the recipient of the 2014 IEEE Signal Processing Society Meritorious Service Award.